Magnetic phase diagram of Ru-doped $Sm_{1-x}Ca_xMnO_3$ manganites: Expansion of ferromagnetism and metallicity

C. Martin,* A. Maignan, M. Hervieu, C. Autret, and B. Raveau
Laboratoire CRISMAT, ISMRA, 6 Boulevard du Maréchal Juin, 14050 CAEN Cedex, France

D. I. Khomskii
Solid State Physics Laboratory, Materials Science Centre, University of Groningen, Nijenborgh 4, 9747 AG Groningen, The Netherlands
(Received 26 July 2000; revised manuscript received 7 November 2000; published 28 March 2001)

The substitution of ruthenium for manganese has been studied in the $Sm_{1-x}Ca_xMnO_3$ series, leading to a magnetic (T vs x) phase diagram where a large region of ferromagnetic metallic phases appears. These results are compared with those obtained by chromium doping in the same system, showing the much stronger effect of ruthenium. Other lanthanide series have also been characterized in order to investigate the size effect in the ruthenium doped compounds. A comprehensive magnetic study by powder neutron diffraction has been performed on the $Sm_{0.2}Ca_{0.8}Mn_{0.9}Ru_{0.1}O_3$ compound in connection with the phase separation evidenced by the susceptibility measurements. Finally, models for orbital and spin ordering are proposed to explain the Cr and Ru induced ferromagnetism and metallicity.

DOI: 10.1103/PhysRevB.63.174402 PACS number(s): 75.30.Mb, 71.30.+h, 75.25.+z, 68.37.−d

INTRODUCTION

Soon after the discovery of the field induced insulator-metal (IM) transition in $Pr_{0.5}Sr_{0.5}MnO_3$,[1] it was shown that the size of the *A*-site cation dramatically influences such a transition and, by the way, the colossal magnetoresistance (CMR) properties of the manganites.[2–4] A striking example is given by the charge ordered phase $Pr_{0.5}Ca_{0.5}MnO_3$ which was reported to be stable up to 27 T, and by the fact that no spontaneous IM transition is observed in the $Pr_{1-x}Ca_xMnO_3$ system in the absence of magnetic field for any x,[5] in contrast to the $Pr_{1-x}Sr_xMnO_3$ system. The existence of IM transition in Cr-doped manganites $Pr_{0.5}Ca_{0.5}Mn_{1-x}Cr_xO_3$, in the absence of magnetic field[6] is very attractive since it shows the possibility to modify dramatically the magnetic phase diagram of the manganites, by doping the Mn sites with a magnetic cation. It has indeed been proposed that such induced CMR properties result from the competition between ferromagnetic metallic and antiferromagnetic (AFM) insulating domains.[7–9] Among the magnetic cations capable to induce metallicity and ferromagnetism in manganites, ruthenium appears as most promising due to its ability to adopt two valencies, Ru^{4+} and Ru^{5+}, which can both participate to strong superexchange ferromagnetic interactions with Mn^{3+}.[10–13] On the basis of these results, we have explored the Ru doping of the system $Sm_{1-x}Ca_xMnO_3$, for which ferromagnetic metallic state has only been observed in the ''cluster glass'' domain (for $0.9 \leqslant x < 1$) due to the small size of the *A*-site cations.[14] We show that the large AFM charge ordered region observed in the undoped system ($0.40 < x < 0.80$) is replaced by a ferromagnetic metallic (FMM) state, with high T_C up to 235 K. A comparison is made with the Cr-doped system[15] which exhibits a much smaller FMM region, and much lower T_C. We propose a model of orbital and spin ordering which may explain these magnetic properties and the different behavior of ruthenium and chromium.

EXPERIMENT

The different samples of the system $Sm_{1-x}Ca_xMn_{1-y}Ru_yO_3$ were prepared by solid state reaction in air at 1500 °C, starting from the stoichiometric mixtures of the oxides Sm_2O_3, CaO, MnO_2, and RuO_2 according to the procedure previously described.[11–13]

The purity and crystallographic nature of the perovskite were checked by x-ray diffraction and by transmission electron microscopy (TEM) coupled with energy dispersive spectroscopy (EDS). Electron diffraction (ED) studies were carried out with JEOL. 200CX and JEOL 2010 electron microscopes. The reciprocal space was reconstructed by tilting around the crystallographic axes, at room temperature (RT) and at 92 K. The high-resolution electron microscopy was carried out with a TOPCON 002B microscope ($V = 200$ kV, $Cs = 0.4$ mm). Neutron powder diffraction experiments have been performed by using the G41 diffractometer in LLB-Saclay ($\lambda = 2.4266$ Å). The patterns were recorded over an angular range $17° \leqslant 2\theta \leqslant 97°$ by increasing the temperature from 1.5 K to room temperature by steps of 5 K. The samples used for this structural study have been prepared with Sm^{152}. The data have been analyzed with the Rietveld method using the FULLPROF program.

The T dependence of the magnetization (M) was registered with a vibrating sample magnetometer, warming from 4.2 to 300 K in 1.45 T or in 10^{-3} T after zero field cooling (ZFC). The resistivity data were collected with a four-probe method, cooling the bars from 400 to 5 K either in the absence of magnetic field (ZFC) or in 7 T (FC).

The phase diagrams have been built by using the magnetization values recorded in 1.45 T (ZFC) at 4.2 K and the T_C determined from the inflection points of the $M(T)$ curves collected in 10^{-3} T for the Ru-doped series. The T_C's values for the undoped and Cr-doped series were deduced from $M(T)$ curves collected in 1.45 T. It should be emphasized that the T_C's of the Ru-doped compositions depend on the applied magnetic field value in contrast to the undoped and

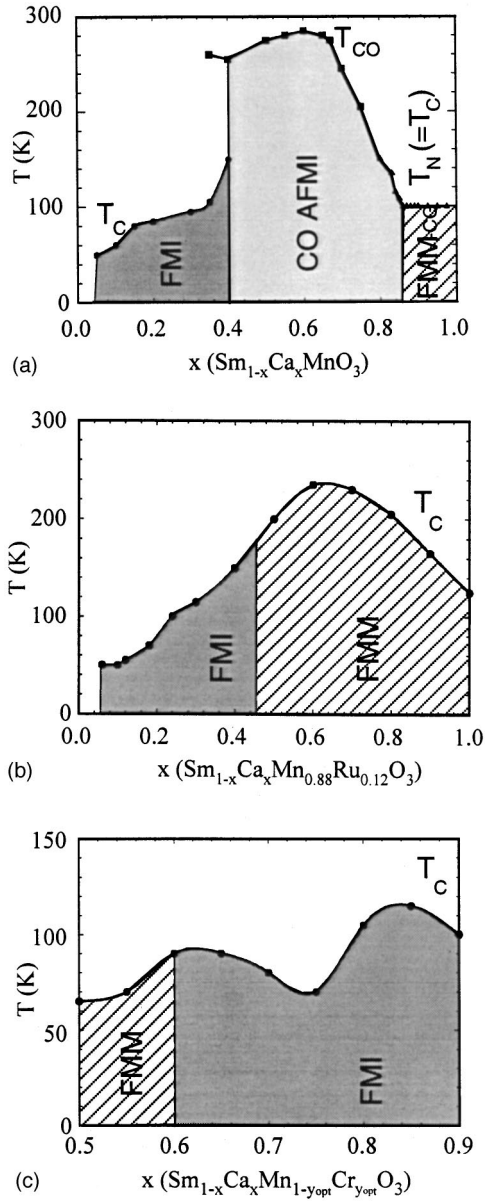

FIG. 1. (a) Phase diagram of the $Sm_{1-x}Ca_xMnO_3$ series from Ref. 14. ●, ■, and ▲ are for T_C, T_{CO}, and T_N, respectively. *I* and *M* referred to insulator and metal arbitrarily defined from the resistivity value at 10 K, $>10^4\,\Omega$ cm and $<10^0\,\Omega$ cm for *I* and *M*, respectively. (b) The same for $Sm_{1-x}Ca_xMn_{0.88}Ru_{0.12}O_3$. (c) The same for $Sm_{1-x}Ca_xMn_{1-y}Cr_yO_3$ from Ref. 15.

Cr-doped series. The anomalous nature of the FM state of the Ru-doped $Sm_{1-x}Ca_xMnO_3$ series is discussed later.

RESULTS AND DISCUSSION

Investigations in the $Sm_{1-x}Ca_xMn_{1-y}Ru_yO_3$ system

The consideration of the magnetic phase diagram of the undoped manganites $Sm_{1-x}Ca_xMnO_3$ [Fig. 1(a)] shows that the coexistence of ferromagnetism and metallicity is barely seen in this system, in agreement with the small size of the Sm^{3+} and Ca^{2+} cations. The major part of the diagram, $0.40 \leqslant x \leqslant 0.80$, shows at low *T* a charge ordered antiferromagnetic insulating (AFMI) state, with a T_{CO} maximum of 280 K for $Sm_{0.4}Ca_{0.6}MnO_3$. In the Mn^{3+} rich region, $x < 0.40$, ferromagnetism is observed, but no metallicity is detected, in contrast to the large *A*-site size systems like $Pr_{1-x}Sr_xMnO_3$.[14] In this ferromagnetic insulating (FMI) region, T_C increases with *x*, from ≈50 K for $x=0.05$ to ≈100 K for $x=0.35$. For all compositions corresponding to $0 \leqslant x \leqslant 0.80$, the resistivity ($\rho$) at low temperature (10 K) is always very high ($>10^4\,\Omega$ cm) and is thus called ''insulating.'' Coexistence of ferromagnetism and metallicity is only observed in the cluster-glass (CG) region, i.e., for $x \approx 0.9$.[16] The latter exhibit $\rho_{10\,K}$ values of 10^{-2}–$10^{-3}\,\Omega$ cm, i.e., values close to the Mott criterion for ''bad'' metals. In the following, all samples characterized by $\rho_{10\,K} < 10^0\,\Omega$ cm will be referred to as ''metals'' in contrast to the insulating compositions (such as $0 \leqslant x \leqslant 0.80$). Starting from the previous results obtained by Ru doping of manganites,[10–13] we have first explored the possibility to enhance ferromagnetism and to induce metallicity selecting three compositions, $x=0.30$, 0.60, and 0.90 and varying *y* in the range 0–0.15.

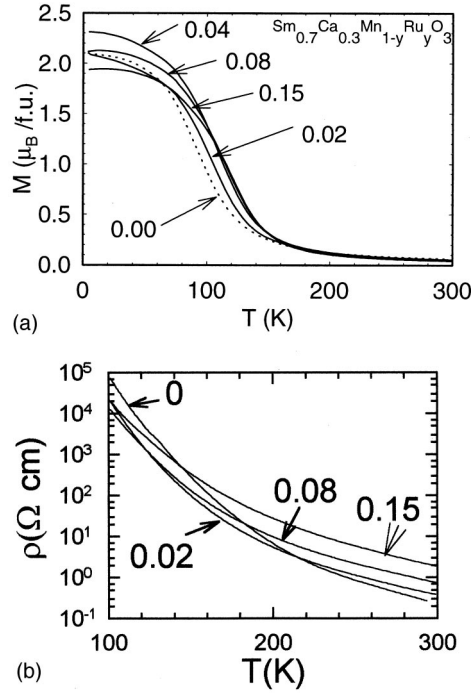

FIG. 2. (a) Temperature dependence of the magnetization (*M*) of the phases $Sm_{0.7}Ca_{0.3}Mn_{1-y}Ru_yO_3$ (ZFC, $\mu_0 H = 1.45$ T). The *y* values are labeled. (b) Temperature dependence of the resistivity (ρ) for the same series; the values are collected upon cooling from 400 K.

The $M(T)$ curves of the $Sm_{0.7}Ca_{0.3}Mn_{1-y}Ru_yO_3$ phases [Fig. 2(a)] show that the magnetization values at 4.2 K, ranging from 1.9 to $2.3\mu_B$, increase only slightly with the Ru content, from $y=0$ to 0.04, the theoretical value being not reached under 1.45 T. The T_C values, deduced from the inflection on the derived curves [$dM/dT = f(T)$] of the $M(T)$ curves collected in 10^{-3} T, slightly increase with the Ru content from $T_C = 95$ K for $y=0$ to 115 K for $y=0.12$. The resistivity measurements show that, whatever the Ru content, the compounds $Sm_{0.7}Ca_{0.3}Mn_{1-y}Ru_yO_3$ [Fig. 2(b)] are insu-

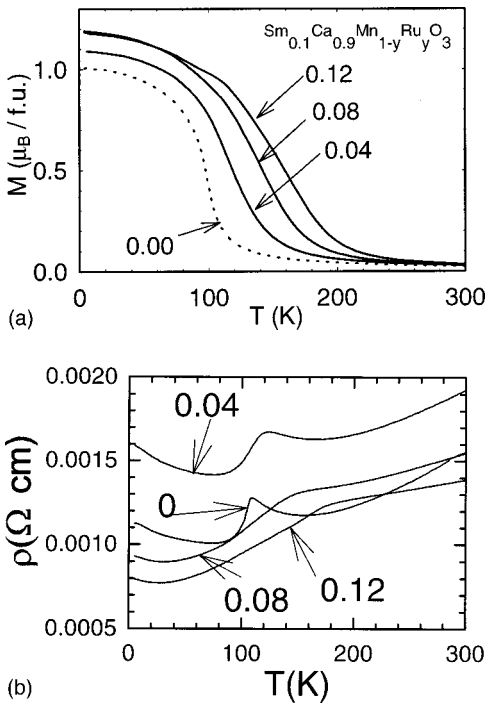

FIG. 3. (a) $M(T)$ curves for $Sm_{0.1}Ca_{0.9}Mn_{1-y}Ru_yO_3$ (ZFC; $\mu_0 H = 1.45$ T). (b) $\rho(T)$ curves for the same system.

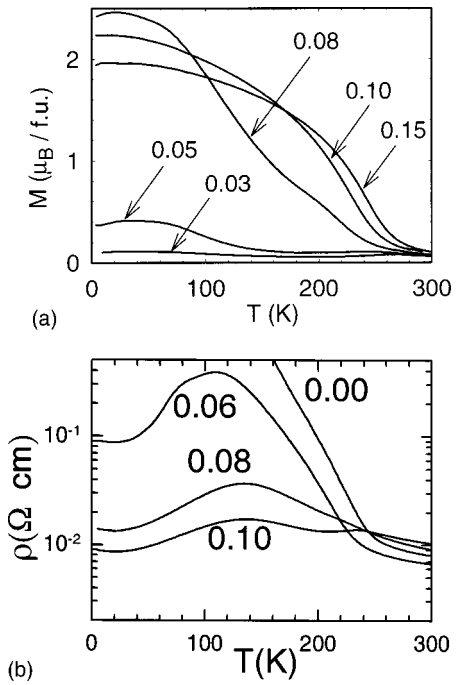

FIG. 4. (a) $M(T)$ curves of $Sm_{0.4}Ca_{0.6}Mn_{1-y}Ru_yO_3$ (ZFC; $\mu_0 H = 1.45$ T). (b) $\rho(T)$ curves for this system.

lators $[d\rho/dT < 0]$ with too high $\rho_{10\,K}$ values to be measurable. Thus the substitution of Ru for Mn in $Sm_{0.7}Ca_{0.3}Mn_{1-y}Ru_yO_3$ only expands the FMI state towards higher temperatures.

For the electron doped manganites $Sm_{0.1}Ca_{0.9}Mn_{1-y}Ru_yO_3$, the magnetization values [Fig. 3(a)] at 5 K are significantly smaller than for the hole doped sample $x = 0.3$, reaching only $1.2\mu_B$, and do not vary significantly with the Ru content. In contrast, the T_C values increase considerably with the Ru content, going from 100 K for $y = 0$ to 165 K for $y = 0.12$. The corresponding resistivity curves [compare $y = 0$ and $y = 0.12$ in Fig. 3(b)] show that the metal-metal transition at $T - T_C \sim 100$ K already observed for the pristine compound is maintained by Ru doping, but the transition temperature increases with the Ru content.

In fact, the most spectacular effect is observed for the $Sm_{0.4}Ca_{0.6}Mn_{1-y}Ru_yO_3$ series. Starting from the antiferromagnetic (AFM) charge ordered pristine phase ($y = 0$) with $T_{CO} = 250$ K, the $M(T)$ curves of this series [Fig. 4(a)] show that FM grows rapidly with Ru content, leading to a magnetic moment of $2.2\mu_B$ at 5 K for $y = 0.10$ and a T_C close to 240 K. This dramatic tendency of ruthenium to destroy charge ordering, and to induce ferromagnetism, was previously shown for $Sm_{0.2}Ca_{0.8}MnO_3$.[13] For the latter manganite, the resistivity exhibits simultaneous M-M and PM-FM transitions as shown further in Fig. 6 for $Sm_{0.2}Ca_{0.8}Mn_{0.9}Ru_{0.1}O_3$. A similar trend is observed for $Sm_{0.4}Ca_{0.6}Mn_{1-y}Ru_yO_3$ (Fig. 4), but the ρ change at T_C is much smaller than the one observed below the broad maximum which develops well below T_C. This second broad maximum was previously interpreted in terms of competition between ferromagnetic metallic (FMM) and antiferromagnetic insulating (AFM) domains[11,13] in the frame of a percolation. The second broad maximum would correspond to the percolation threshold between FMM regions which occurs far below T_C due to the growing of these clusters as T decreases.

Magnetic phase diagram of the $Sm_{1-x}Ca_xMn_{0.88}Ru_{0.12}O_3$ system

Taking into consideration the above results and those previously obtained for the Ru-doped manganites $Sm_{0.4}Ca_{0.6}MnO_3$ and $Sm_{0.2}Ca_{0.8}MnO_3$,[11–13] the magnetic phase diagram has been established for the system $Sm_{1-x}Ca_xMn_{0.88}Ru_{0.12}O_3$ [Fig. 1(b)]. This Ru level of substitution was chosen according to the two antagonistic effects: T_C increases as the Ru content (y) increases but the homogeneity of the Ru distribution in the matrix decreases for y values beyond 0.12–0.15, depending on the Mn valency (x value). The modification of the magnetic phase diagram with respect to the $Sm_{1-x}Ca_xMnO_3$ system [Fig. 1(a)] is considerable. The $x < 0.45$ part of the diagram remains FMI with Ru doping, but differs from the undoped one by the higher T_C values observed for $x \geqslant 0.3$. The most impressive modification concerns the disappearance of the charge-ordered state by Ru doping, for $0.45 \leqslant x < 0.80$, at the benefit of a FMM state with very high T_C going through a maximum of 235 K around $x \sim 0.6$ [Fig. 1(b)]. Thus, the doping with ruthenium tends to destroy the charge ordering and to induce an extremely wide FMM region, x ranging from 0.45 to 1 [Fig. 1(b)].

This effect of Ru doping is still more spectacular than that previously observed for chromium doping.[15] In the case of the Cr-doped $Sm_{1-x}Ca_xMnO_3$ system, depending on x, dif-

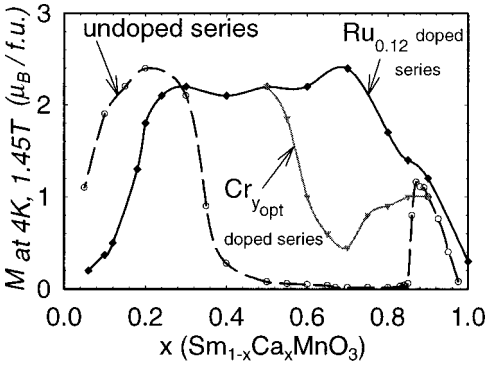

FIG. 5. x dependence of the magnetization (M) at 4.2 K for the $Sm_{1-x}Ca_xMn_{1-y}Me_yO_3$ samples with Me=Ru(◆) and Me=Cr(▼). (○): pristine samples ($y=0$) ($\mu_0 H=1.45$ T).

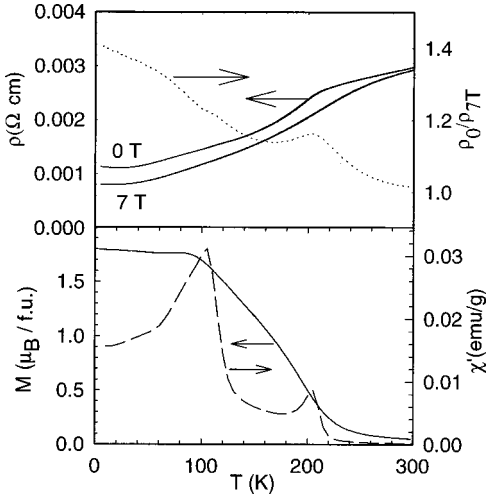

FIG. 6. $Sm_{0.2}Ca_{0.8}Mn_{0.9}Ru_{0.1}O_3$: $\rho(T)$ (left axis) and resistivity ratio curves (right axis) in the upper part and $M(T)$ (ZFC; $\mu_0 H=1.45$ T; left axis) and $\chi'(T)$ ($h_{dc}=0$; $h_{ac}=3$Oe, $f=100$ Hz; right axis) in the lower part.

ferent optimal values of the Cr level are required to induce a maximum of magnetization. The corresponding phase diagram established for $0.5 \leqslant x \leqslant 0.9$ [Fig. 1(c)] shows that chromium is much less efficient for inducing ferromagnetism and metallicity. However it allows CMR to be obtained in this composition range. Although charge ordering tends to be destroyed for all this Mn^{4+} rich region, the FMM state is much more narrow for Cr than for Ru, x ranging from 0.5 to 0.6, and instead a FMI state appears for x ranging from 0.6 to 0.9. Moreover, the Curie temperatures are much smaller than those observed for Ru: they range indeed from 65 to 115 K, to be compared to 100–235 K for Ru-doped manganites. This greater efficiency of ruthenium compared to Cr to induce ferromagnetism is corroborated by the evolution of the magnetic moment at 4.2 K versus x (Fig. 5) which is systematically higher for Ru than for Cr doping for $x>0.50$.

Nature of the FMM state: Magnetic phase separation

The fact that the magnetic moments at low temperature do not reach the theoretical values even under higher magnetic fields (5 T with our magnetometer) and also that the $\rho(T)$ curves in several cases show a second bump at low temperature suggest that the FMM state in all these oxides is anomalous [see Fig. 6 the broadness of the $M(T)$ curve of $Sm_{0.2}Ca_{0.8}Mn_{0.9}Ru_{0.1}O_3$ recorded in 1.45 T]. This behavior has also been revealed by the ac magnetic susceptibility (ac-χ) measurements, as a function of temperature, in the case of the $Sm_{0.2}Ca_{0.8}Mn_{1-y}Ru_yO_3$ series, showing the existence of two maxima, for instance at 205 and 105 K for $y=0.1$ (Fig. 6). This may point out that the system is actually inhomogeneous or ''phase separated.'' [13] We therefore have undertaken a structural and magnetic study of $Sm_{0.2}Ca_{0.8}Mn_{0.9}Ru_{0.1}O_3$ combining electron microscopy and powder neutron diffraction.

The reconstruction of the reciprocal space at room temperature confirmed the orthorhombic cell with the *Pnma*-type distortion. The high resolution electron microscopy images, recorded along the different crystallographic axes, show that the ruthenium species are statistically distributed in the octahedral framework. This is corroborated by the coupled EDS analyses which show an homogeneous Ru content corresponding to the nominal one (y). The electron diffraction investigation has been then carried out by cooling the sample down to 92 K. No significant structural event is detected in this temperature range. The large majority of the crystallites exhibit a system of sharp reflections without any splitting nor satellites which would indicate monoclinic distortion or charge ordering phenomena, respectively, as observed for the $y=0.06$ and 0.08 samples.[17] This is illustrated in Fig. 7(a) which displays a typical [010]ED pattern recorded at 92 K. A unique *Pnma* space group is thus exhibited by all the studied crystallites so that no phase separation could be claimed from electron microscopy.

In contrast, the powder neutron diffraction, details of which will be published elsewhere, as well as the magnetic and transport properties (Fig. 6) clearly show the phase separation at low temperature. The $Sm_{0.2}Ca_{0.8}Mn_{0.9}Ru_{0.1}O_3$ compound exhibits a *Pnma* structure in the whole temperature range (from 15 K to room temperature) as mentioned previously in the electron microscopy. The lattice parameters refined at room temperature are close to those of $Sm_{0.3}Ca_{0.7}MnO_3$,[18] in agreement with the increase of the Mn^{3+}/Mn^{4+} ratio compared to $Sm_{0.2}Ca_{0.8}MnO_3$, which is induced by the Ru^{5+} substitution for Mn^{3+}/Mn^{4+}, but the cell of the Ru-doped sample is slightly less distorted. At liquid helium temperature, the magnetic and crystalline structures are similar to the $Sm_{0.1}Ca_{0.9}MnO_3$ ones,[19] i.e., the *Pnma* crystal structure is associated with an antiferromagnetic *G*-type phase and a ferromagnetic component. But the evolution with temperature is different for both manganites: for $Sm_{0.1}Ca_{0.9}MnO_3$, T_N and T_C are very close (around 110 K), in contrast to the transition temperatures of $Sm_{0.2}Ca_{0.8}Mn_{0.9}Ru_{0.1}O_3$ which differ by ~100 K with $T_C \approx 210$ K and $T_N \approx 100$ K as shown in Fig. 7(b) from the T dependence of the refined magnetic moments. The latter temperatures corroborate those determined from the two peaks of the $\chi'(T)$ curves (Fig. 6). Note that the Ru-doped sample differs strongly from the undoped one $Sm_{0.2}Ca_{0.8}MnO_3$, since it exhibits no phase separation but only a monoclinic

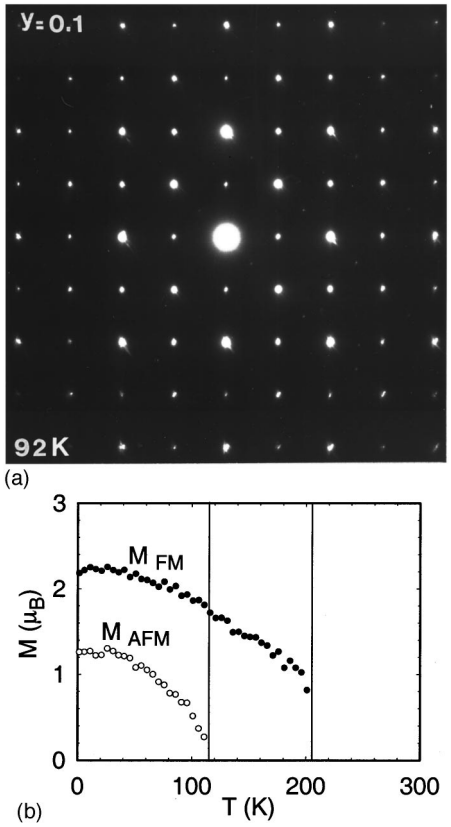

FIG. 7. (a) ED pattern of $Sm_{0.2}Ca_{0.8}Mn_{0.9}Ru_{0.1}O_3$ recorded at 92 K. (b) Temperature dependence of the magnetic moments of the antiferromagnetic (AFM) and the ferromagnetic (FM) components for the same compound deduced from the refinements of the powder neutron diffraction data.

distortion ($P2_1/m$ space group), associated with a *C*-type AFM state, below 150 K.[20] This neutron diffraction study evidences thus a clear difference between T_C and T_N leading to a magnetic phase separation (AFM and FM) at low temperature. However, in the absence of high resolution synchrotron powder diffraction for $Sm_{0.2}Ca_{0.8}Mn_{0.9}Ru_{0.1}O_3$, the coexistence of two different phases crystallizing in the same space group but with only slightly different cell parameters cannot be ruled out.

Extension to other lanthanides: Size effect

The above results can be extended to other lanthanides, as shown from the $M(T)$ curves of $Ln_{0.5}Ca_{0.5}MnO_3$ manganites doped with 5% ruthenium and chromium [Fig. 8(a)]. Both Ru and Cr doping promote ferromagnetism in the $Ln_{0.5}Ca_{0.5}MnO_3$ manganites. However it is remarkable, that starting from an antiferromagnetic pristine phase, the magnetic moment induced by Ru doping increases spectacularly with the size of the *A*-site cation from $0.7\mu_B$ for Sm or Ho to $\approx 3\mu_B$ for Nd, Pr, and La. A similar effect is also observed for Cr doping. This effect is closely related to the fact that the stability of the charge-ordering decreases at the benefit of FM as the size of the *A*-site cation increases.[21,22] In a similar way, T_C increases with the size of the *A*-site cation, whatever

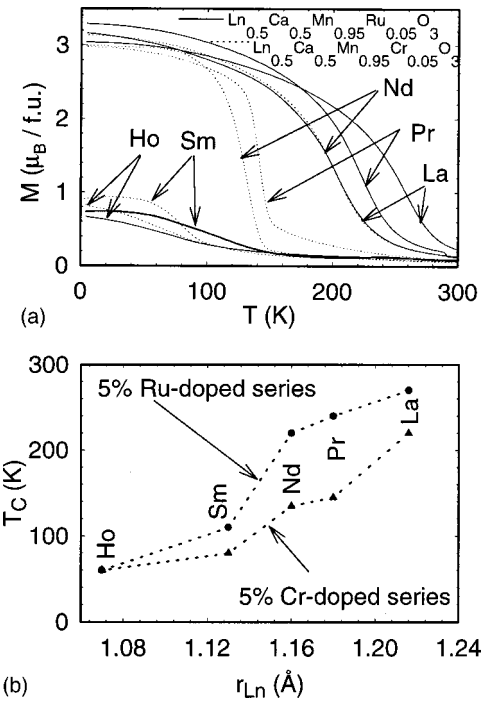

FIG. 8. (a) $M(T)$ curves of 5% doped $Ln_{0.5}Ca_{0.5}MnO_3$ manganites with Ru (solid lines) and Cr (dotted lines) (ZFC; $\mu_0 H = 1.45$ T). (b) T_C as a function of the Ln size for the 5% doped [(Cr (from Ref. 21) and Ru)] $Ln_{0.5}Ca_{0.5}MnO_3$ manganites.

the doping cation, Ru or Cr [Fig. 8(b)]. Note also that Ru is significantly more efficient than Cr for the large Ln size.

Models for orbital and spin ordering in Ru and Cr doped manganites

Considering the above results and those previously obtained for chromium, we have to explain why both cations induce ferromagnetism and metallicity and why ruthenium is spectacularly more efficient than chromium. Let us take for the elaboration of our model, the doping of the charge ordered CE-type oxides $Ln_{0.5}Ca_{0.5}MnO_3$, whose magnetic structure projected in 2D [Fig. 9(a)] consists of FM zigzag chains of Mn^{3+}/Mn^{4+} cations, the coupling between chains being antiferromagnetic. This drawing corresponds to the (*a*, *c*) plane in the *Pnma* space-group, the *b* direction being perpendicular to this plane.

For charge reasons, the doping with chromium in the CO structure corresponds to the local substitution of one Cr^{3+} for one Mn^{3+}. As previously shown from circular dichroism measurements,[23] Cr^{3+} is antiferromagnetically coupled with all its nearest neighbors. Thus the Cr^{3+} species can sit in one zigzag chain without disturbing the spin orientation of the two neighboring zigzag provided its spin orientation is opposite to them [Fig. 9(b)]. Then the spin orientation of its two Mn^{4+} neighbors within its own chain will be reversed to be antiferromagnetically coupled with Cr^{3+}, and finally the spins of all the other Mn^{3+}/Mn^{4+} species of this ''Cr-zigzag'' will be reversed in order to keep the ferromagnetic coupling within the chain [dark arrows on Fig. 9(b)]. Thus, each time one Cr is introduced in a zigzag chain, the spins of

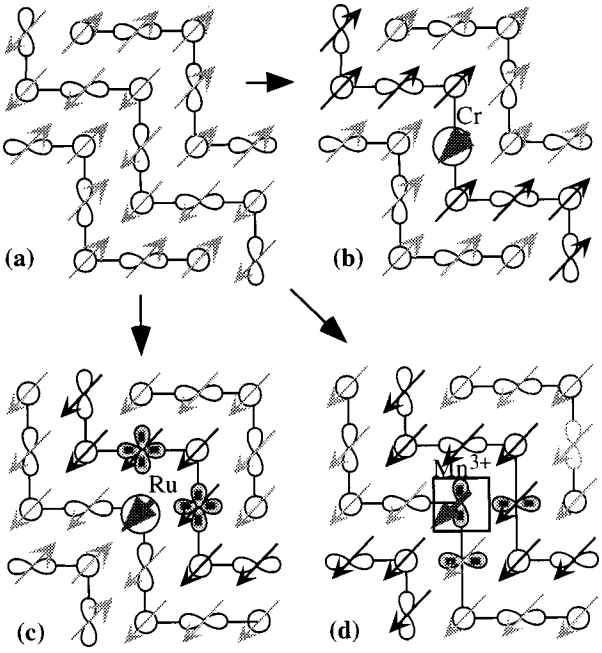

FIG. 9. Creation of FM regions in the (010) layer of the CE-type structure (a) by Cr doping (b), Ru doping (c), and additional Mn^{3+} (d). The black arrows correspond to the spins which have been reversed, whereas the shaded orbitals are rotated (d_z^2 or $d_{x^2-y^2}$ ones). Open circles correspond to Mn^{4+} sites and e_g orbitals are located on Mn^{3+} sites.

the Mn^{3+}/Mn^{4+} of this chain can be reversed by ''domino effect'' leading to triple ferromagnetic chains. Of course, further away along the zigzags, the original spin ordering should be restored.

Yet another factor favoring ferromagnetism is that the spin down Cr^{3+} ions interact antiferromagnetically not only with the surrounding Mn ions in the (*a, c*) plane but also with the Mn in the planes above and below, thus providing some ferromagnetic coupling between the planes. Due to the mechanisms described above, each Cr would induce an elliptic ferromagnetic microregion. This explains the appearance of both ferromagnetism and metallicity when a sufficient level of Cr^{3+} is introduced on the Mn sites. Nevertheless, the Cr^{3+} e_g states are rather high with respect to manganese, and not reactively available for hybridization and for participating to the band formation. Consequently, the contribution of Cr to the increase of conductivity is not very strong in a first step for low chromium levels, and metallicity is only reached for higher Cr content when the major part of the structure is melted into the ferromagnetic state.

In the case of ruthenium doping, the substitution of manganese can be made either by Ru^{4+} or Ru^{5+} species, the latter being more probable due to synthesis conditions,[24,25] though a valence fluctuation according to the equilibrium $Mn^{3+}+Ru^{5+} \leftrightarrow Mn^{4+}+Ru^{4+}$ is most likely. Let us first consider the Ru^{4+} doping, which substitutes for Mn^{4+} in low spin, t_{2g}^4 configuration. Ruthenium is more covalent than chromium and most probably the e_g states of ruthenium should participate to the band formation and contribute to make it broader. Thus Ru and Mn are FM coupled. The

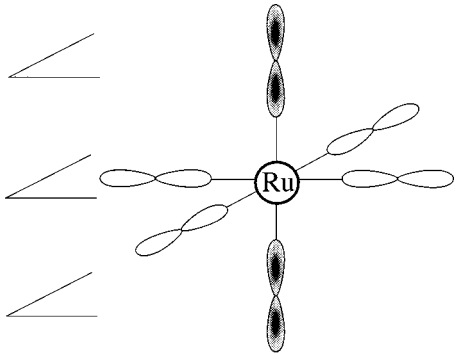

FIG. 10. Introduction of two additional Mn^{3+} in the (010) planes above and below Ru^{5+}, with their d_z^2-like orbital (hatched) directed toward Ru^{5+}, leading to an orbital polaron.

introduction of one Ru^{4+} species on one Mn^{4+} site will not change the orientation of the Mn^{3+} orbital of its zigzag chain, and in this chain the Ru^{4+} and Mn^{3+} species will remain FM coupled. In contrast the orbitals of the two Mn nearest neighbors of Ru belonging to the adjacent chain may rotate [Fig. 9(c)] so that they all point towards Ru, to make the optimal use of strong Mn-Ru hybridization, or could rather become x^2-y^2-like. Then the spins of these Mn^{3+} ions will be reversed and become FM coupled with Ru^{4+}. Finally this adjacent zigzag chain [dark arrows in Fig. 9(c)] would reverse its spins by ''domino effect'' in order to keep FM coupling between its Mn^{3+}/Mn^{4+} cations. From this model, it can be seen that differently from Cr doping, Ru doping involves conduction via Ru itself and that the rotated d_z^2 orbitals or the $d_{x^2-y^2}^2$ ones provide new conduction paths between neighboring zigzag FM chains, so that hopping is no more forbidden. Thus the connection between the zigzag chains is better than for chromium.

The same model of the orbital rotation and creation of FM can also be proposed and will even be more efficient for Ru^{5+}. But, in contrast to Ru^{4+},Ru^{5+} doping introduces extra Mn^{3+} according to the substitution $2Mn^{4+}=Ru^{5+}+Mn^{3+}$. This valency effect will in fact reinforce the FM coupling and metallicity. The introduction of Ru^{5+} on one site will induce FM coupling and metallicity within the (010) plane according to the mechanism previously described for Ru^{4+}. But simultaneously the additional Mn^{3+} can occupy the former Mn^{4+} site close to Ru^{5+} in an adjacent (010) layer and will orient its d_z^2 orbital towards Ru^{5+}, leading to an ''orbital polarons'' schematically shown in Fig. 10, as in the model recently elaborated.[26] Besides the modification in the (*a, c*) plane, a FM coupling appears thus between the two (010) planes. An electronic fluctuation along the ''Mn^{3+}-O-Ru^{5+}-O-Mn^{4+}'' bond is also possible which makes that three (010) planes could be ferromagnetically coupled along the *b* direction by doping with Ru^{5+} species (Fig. 11).

Finally, extra Mn^{3+} can also participate to the enhancement of ferromagnetism even if it is not close to Ru. The introduction of one additional Mn^{3+} species on one Mn^{4+} site of the CE-type structure leads to formation of ferromagnetic cluster similar to the orbital and FM spins arrangements

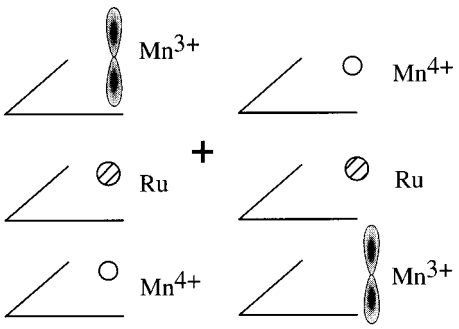

FIG. 11. Introduction of one additional Mn^{3+} and the possible electronic fluctuations along the ''Mn-O-Ru-O-Mn'' bond leading to the FM coupling of three manganese (101) planes.

observed in the FM (001) layer of the *A*-type AFM $LaMnO_3$, see Fig. 9(d), with the corresponding flipping of the spins of two zigzags [blacks arrows in Fig. 9(d)]. Thus this extra Mn^{3+}, introduced by valency effect of Ru^{5+}, generates orbitally ordered FM regions, even in the regions where Ru^{5+} is absent. It is possible that the last factor also explains the tendency towards phase separation into CO/CE regions and FM clusters for the $Ln_{1-x}Ca_xMnO_3$ phase with $x<0.5$ but not for $x>0.5$ which remains purely CO. An alternative possibility (not drawn here) is that this extra Mn^{3+} will have d_z^2 occupation (perpendicular to the plane), in which case the situation will be similar to that of Ru^{5+} with, as a consequence, formation of a similar ferromagnetic cluster extended also in the *b* direction.

CONCLUSION

An anomalous ferromagnetic metallic state can be induced by Ru doping in the charge ordered manganites ($Sm_{1-x}Ca_xMn_{1-y}Ru_yO_3$) corresponding to x in the range 0.45 to 1, i.e., for Mn valency in between 3.45 and 4. Ruthenium is found to be much more efficient than chromium, since higher T_C's and a much broader region of a metallic regime are reached with the substitution of the former. The anomalous ferromagnetic state and the percolative transport mechanism points out towards a phase segregation which has been probed by powder neutron diffraction. The present Ru effect is explained in terms of orbital reorientation and spin reversal in the antiferromagnetic structures resulting from a ferromagnetic coupling between Ru^{4+}/Ru^{5+} and Mn^{3+}. Moreover, the possibility for Ru to exhibit a mixed-valency introduces Mn^{3+}/Mn^{4+} electronic fluctuations around Ru which may strongly enhance the formation of ferromagnetic metallic clusters.

*Corresponding author. FAX: 33 2 31 95 16 00. Email address: christine.martin@ismra.fr

[1] Y. Tomioka, A. Asamitsu, Y. Moritomo, and Y. Tokura, Phys. Rev. Lett. **74**, 5108 (1995).
[2] R. Mahesh, R. Mahendiran, A. K. Raychaudhuri, and C. N. R. Rao, J. Solid State Chem. **114**, 297 (1995); **120**, 204 (1995).
[3] H. Y. Hwang, S. W. Cheong, P. G. Radaelli, M. Marezio, and B. Batlogg, Phys. Rev. Lett. **75**, 914 (1995).
[4] A. Maignan, Ch. Simon, V. Caignaert, and B. Raveau, Solid State Commun. **96**, 623 (1995).
[5] M. Tokunaga, N. Miura, Y. Tomioka, and Y. Tokura, Phys. Rev. B **57**, 5259 (1998).
[6] B. Raveau, A. Maignan, C. Martin, and M. Hervieu, J. Solid State Chem. **130**, 162 (1997).
[7] Y. Moritomo, A. Machida, S. Mori, N. Yamamoto, and A. Nakamura, Phys. Rev. B **60**, 9220 (1999); T. Katsufuji, S. W. Cheong, S. Mori, and C. H. Chen, J. Phys. Soc. Jpn. **68**, 1090 (1999).
[8] T. Kimura, Y. Tomioka, and Y. Tokura, Phys. Rev. Lett. **83**, 3940 (1999).
[9] R. Mahendiran, M. Hervieu, A. Maignan, C. Martin, and B. Raveau, Solid State Commun. **114**, 429 (2000).
[10] P. V. Vanitha, A. Arulraj, A. R. Raju, and C. N. R. Rao, C. R. Acad. Sci., Ser. IIc **2**, 595 (1999).
[11] B. Raveau, A. Maignan, C. Martin, R. Mahendiran, and M. Hervieu, J. Solid State Chem. **151**, 330 (2000).
[12] B. Raveau, A. Maignan, C. Martin, and M. Hervieu, Mater. Res. Bull. **35**, 1579 (2000).
[13] C. Martin, A. Maignan, M. Hervieu, B. Raveau, and J. Hejtmanek, Eur. Phys. J. B **16**, 469 (2000).
[14] C. Martin, A. Maignan, M. Hervieu, and B. Raveau, Phys. Rev. B **60**, 12 191 (1999).
[15] A. Maignan, C. Martin, F. Damay, M. Hervieu, and B. Raveau, J. Magn. Magn. Mater. **188**, 185 (1998).
[16] A. Maignan, C. Martin, F. Damay, B. Raveau, and J. Hejtmanek, Phys. Rev. B **58**, 2758 (1998).
[17] M. Hervieu, C. Martin, A. Maignan, and B. Raveau, J. Solid State Chem. **155**, 15 (2000).
[18] M. Hervieu, A. Barnabé, C. Martin, A. Maignan, F. Damay, and B. Raveau, Eur. Phys. J. B **8**, 31 (1999).
[19] C. Martin, A. Maignan, M. Hervieu, B. Raveau, Z. Jirak, M. M. Savosta, A. Kurbakov, V. Trounov, G. André, and F. Bourée, Phys. Rev. B **62**, 6442 (2000).
[20] C. Martin, A. Maignan, M. Hervieu, and B. Raveau (unpublished).
[21] J. Blasco, J. Garcia, J. M. De Teresa, M. R. Ibarra, J. Perez, P. A. Algarabel, C. Marquina, and C. Ritter, J. Phys.: Condens. Matter **9**, 10 321 (1997).
[22] A. Barnabé, M. Hervieu, C. Martin, A. Maignan, and B. Raveau, J. Appl. Phys. **84**, 5506 (1998).
[23] F. Studer, O. Toulemonde, J. B. Goedkoop, A. Barnabé, and B. Raveau, Jpn. J. Appl. Phys., Part 1 **38**, 377 (1999).
[24] P. D. Battle and C. W. Jones, J. Solid State Chem. **78**, 108 (1989).
[25] P. D. Battle, J. C. Gibb, C. W. Jones, and F. Studer, J. Solid State Chem. **78**, 281 (1989).
[26] T. Mizokawa, D. I. Khomskii, and G. A. Sawatzky, Phys. Rev. B **61**, R3776 (2000); M. Paraskevopoulos, J. Hemberger, A. Loidl, A. A. Mukhin, V. Yu. Ivanov, and A. M. Balbashov, cond-mat/9812305 (unpublished); R. Kilian and G. Khaliullin, Phys. Rev. B **60**, 13 458 (1999).